Sensitivity of the Winter-Kennedy method to inlet and runner blade angle change on a Kaplan turbine

To cite this article: B Baidar *et al* 2019 *IOP Conf. Ser.: Earth Environ. Sci.* **240** 022038

IOP Conf. Series: Earth and Environmental Science **240** (2019) 022038 doi:10.1088/1755-1315/240/2/022038

Sensitivity of the Winter-Kennedy method to inlet and runner blade angle change on a Kaplan turbine

B Baidar[1], J Nicolle[2], B K Gandhi[3], M J Cervantes[1]
[1] Department of Engineering Sciences and Mathematics, Luleå University of Technology, Luleå 971 87, Sweden
[2] Institut de recherche d'Hydro-Québec, Varennes, QC J3X 1S1, Canada
[3] Department of Mechanical and Industrial Engineering, Indian Institute of Technology Roorkee, India

E-mail: binaya.baidar@ltu.se

Abstract. The Winter-Kennedy (WK) method is a widely used index testing approach, which provides a relative or index value of the discharge that can allow to determine the on-cam relationship between blade and guide vane angles for Kaplan turbines. However, some discrepancies were noticed in previous studies using the WK approach. In this paper, a numerical model of a Kaplan model turbine is used to study the effects of upstream and downstream flow conditions on the WK coefficients. Experiment on the model turbine is used to validate unsteady CFD simulations. The CFD results show that the inflow condition affects the pressure distribution inside the spiral casing and hence the WK results. The WK coefficients fluctuate with high amplitude - suggesting using a larger sampling time for on-site measurement as well. The study also concludes that to limit the impact of a change in runner blade angle on the coefficients, the more suitable WK locations are at the beginning of the spiral casing with the inner pressure tap placed between stay vanes on the top wall.

1. Introduction

Hydropower is developing in a steady growth trend with 1246 GW global installed capacity by now and 31.5 GW installed in 2016 alone [1]. Most of the new developments are taking place in South America, East Asia and Pacific regions, while major refurbishments and modernization projects are undergoing in North America and Europe. This renewable energy source is among the cheapest renewable energy sources due to its long lifespan and low operating and maintenance cost. The hydro-mechanical parts of the hydropower station generally last for about four decades and then they are either overhauled or replaced, depending on the economic analysis.

Efficiency measurements are usually performed after refurbishments. While it is relatively straightforward to measure efficiency on the high head machines due to several code-accepted absolute methods, like the ones mentioned in the IEC field testing code [2], similar measurements on the low head machines remain a challenge. The main difficulty regarding efficiency lies in the discharge measurement and are linked to the absence of an established flow profile and continuously varying cross-sections at the inlet. Among several relative methods, the Winter-Kennedy (WK) method is widely used to determine the step-up efficiency before and after refurbishment on the low heads. The WK method utilizes features of the flow physics in a curvilinear motion. A pair of differential pressure taps is placed at different radius in a section of the spiral casing (SC). The method follows the relation for the discharge Q as:

$$Q = K_{\mathrm{WK}} \Delta P^{n} \quad (1)$$

where K_{WK} is the WK coefficient and n is an exponent whose value varies from 0.48 to 0.52 [2]. ΔP is the differential pressure between the outer and inner pressure taps placed on the SC. It is also common to install another pair of taps in other radial location and to use the one that provides the best fit with the expected behaviour.

1.1. Previous works

Although the WK method has a very good repeatability, it is known to sometimes produce erroneous results. The possible causes of this behaviour are reviewed by Baidar et al. [3]. The review shows the local flow changes in the SC are mainly attributed to change in inflow conditions, corrosions, surface roughness, or change in geometry. Kercan et al. [4] concluded that the method is unacceptable for guaranteed efficiency measurement because the inlet flow conditions strongly disturb differential pressure measurements, therefore, the authors qualified WK results are unstable and unreliable. The sensitivity of inlet conditions and guide vane opening angle was also presented by Nicolle and Proulx [5]. The authors in [5] showed that sufficient flow homology cannot be always achieved and therefore the WK coefficient changes. A detailed study on how the inlet conditions can change the flow physics and its effect on the WK method is presented by Baidar et al. [6]. As the method relies on the free vortex flow, the centrifugal force should balance the radial pressure gradient. Apart from the centrifugal force, the three-dimensionality flow nature in SC causes the pressure gradient to be balanced due to secondary flows as well. The authors in [6] also show that the most suitable locations for the inner WK tap are at the beginning of SC and between stay vanes to minimize the influence of inflow conditions.

1.2. Scope of the present work

As flow conditions can change due to the presence of upstream geometry, the full turbine model including full penstock and the upper tank was built and simulated. The initial study includes the effect of the upstream geometries on the WK method.

Further, during an experimental campaign [7] following the refurbishment of the runner, a $\sim 2\%$ error was observed while using the same coefficient for the old and new runners. This raises questions on whether the geometry changes downstream of SC can also affect what happens inside the SC. To answer this question, a Computational Fluid Dynamics (CFD) model of a low head Kaplan turbine was built. The downstream geometry change of the runner was approximated by considering the runner at two different blade angles, one is at best efficient point (BEP) and other is at 5° closed position with respect to the BEP point. The case with 5° closed position from the BEP is termed as BEP-5° hereinafter. Therefore, two different propeller configurations were considered for the study allowing two discharge conditions for the same guide vane angle.

2. Test case and numerical model

The turbine of Hölleforsen hydropower plant located in Sweden is considered here. The plant is considered as low head with a head of 27 m and a discharge of 230 m^3/s. The 1:11 scale model of the prototype, which has 0.5 m runner diameter, 4.5 m head, 0.522 m^3/s discharge and 595 rpm rotational speed at its BEP is used in this study. The previously conducted scale model WK experimental data are used to validate the numerical results presented in this study.

2.1. Numerical methods

The computational domain is shown in figure 1. Two turbine models: the full penstock (FP) model and the half penstock (HP) model were developed. The utilization of these models is described afterward. The FP model includes an upper tank whereas the HP model is cut somewhere in the middle of the penstock. The tank in the FP model was also present in the model test rig and was connected to an upper pressure tank, therefore, it doesn't contain free surface. For both models, there are four subdomains: a penstock (full or half) with a semi-spiral casing (SSC), a distributor with 10 stay vanes (SVs) and 24 guide vanes (GVs), a Kaplan runner with 5 blades and an elbow draft tube. The software ICEM CFD was used to create unstructured hexahedral meshes for all the domains.

CFD simulations were performed using ANSYS CFX. The Unsteady-Reynolds-averaged Navier-Stokes (URANS) equations were utilized for the simulations. The 'High Resolution' spatial discretization scheme was used, in which the discretization was achieved by varying the blend factor from 0.0 to 1.0 based on the local solution field. The second order backward Euler scheme was used to discretize time. A mass flow of 522 kg/s was imposed at the inlet of the FP model to study the effect of upstream geometry, whereas the constant total pressure, which approximates a constant head, was used to study the effect of different runner blade angle. For both cases, the outlet was defined as an opening. The convergence criterion on the root mean square (RMS) residual was set to $1e^{-5}$ and various parameters including K_{WK} for all the WK configurations were monitored to ensure convergence.

The runner was in a rotating frame of reference while all other domains were stationary. Therefore, the runner was defined as a rotating domain with a rotational speed of 595 rpm. The general grid interface (GGI) method was used to connect the mesh between the domains. Two transient rotor-stator interfaces were used between stationary and rotating domains. All the simulations were performed using Menter's two-equation shear stress transport (SST) model [8] using automatic wall treatment.

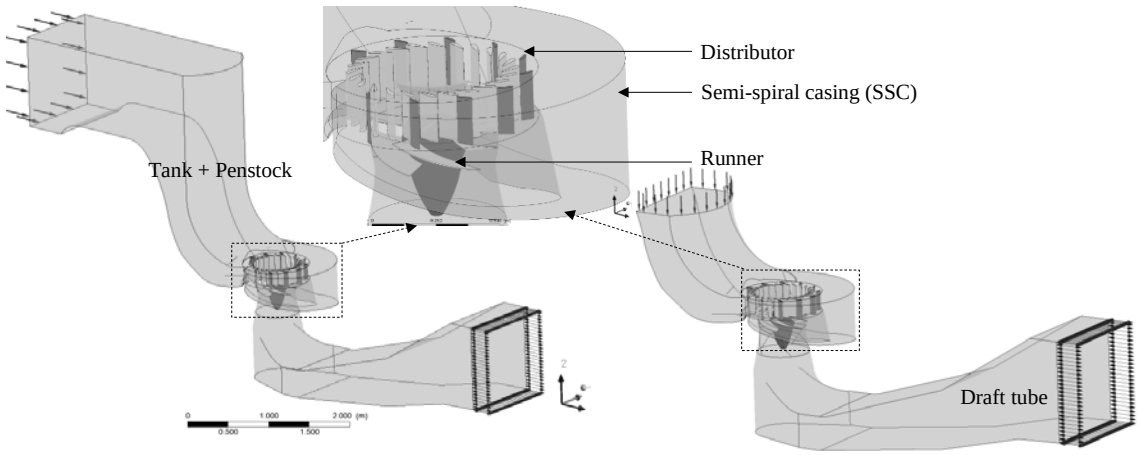

a) Full Penstock (FP) model b) Half Penstock (HP) model

Figure 1. Computational domain: full penstock (FP) model in (*a*) and half penstock (HP) model in (*b*). Both domains consist of a penstock with or without an upper tank, a distributor with 10 SVs and 24 GVs, a runner with 5 blades and an elbow draft tube.

2.2. WK configurations

Seven different circumferential locations of the SSC were chosen from $\theta = 30°$ to 120° and four WK configurations: WK1 to WK4 were considered at each circumferential section. The location of the respective pressure points and the related WK configurations are shown in figure 2.

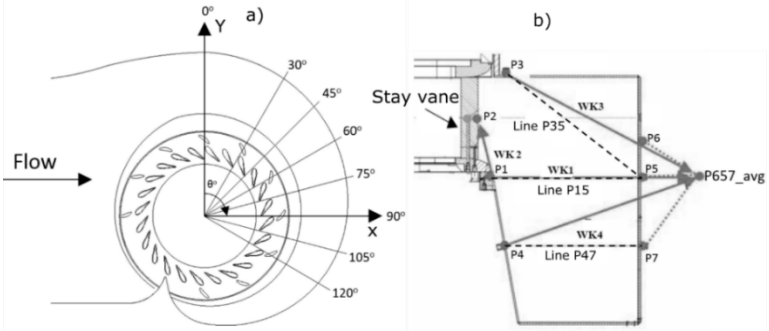

Figure 2. Top view of the SSC showing WK locations from $\theta = 30°$ to 120° used in the study (*a*). A cross-section of the SSC at an angle θ with four WK configurations, WK1 to WK4, are shown in (*b*), where the differential pressures ΔP for WK1, WK3 and WK4 are calculated by the pressure difference between the outer average pressure, i.e. $P657_{avg} = (P5 + P6 + P7)/3$ and the inner pressure point ($P1$, $P3$ or $P4$). WK2 is located at $\theta = 30°$, 60°, 90° and 120° where ΔP is the pressure difference

between $P1$ and $P2$. Further, the lines representing the respective WK configurations are also shown in (b). Figure is adapted from [6].

In this study, the WK coefficient K_{WK} is calculated from equation (1), with the exponent $n = 0.5$. For WK1, WK3 and WK4, the differential pressures ΔP is calculated by the pressure difference between the outer average pressure, i.e. $P657_{avg} = (P5 + P6 + P7)/3$ and the inner pressure point ($P1$, $P3$ or $P4$). The WK2 configuration is located at $\theta = 30°$, 60°, 90° and 120° where ΔP is the pressure difference between $P1$ and $P2$ points. WK2′ is also considered when there is no SV (i.e. at 45°, 75° and 105°). For WK2′ the outer pressure is from $P657_{avg}$ and the inner pressure point is $P2'$, which is located on the top wall of the SC at the same radial distance as $P2$, but in between stay vanes. Further, the pressure difference ΔP is considered per 100 Pa or 1 mbar to calculate the WK coefficients presented.

3. Effect of inlet flow conditions using the Full Penstock (FP) model

3.1. Grid studies

Two sets of grids were considered to study whether the solution was mesh independent. The study involved the FP model shown in figure 1(a) and the grid parameters for Grid 1 (G1) and Grid 2 (G2) shown in table 1.

Table 1. Grid densities used in the study. G1 is finer and G2 is relatively coarse mesh.

Sub-domain	G1 (in million)	G2 (in million)
Penstock + SSC	4.36	2.64
Distributor	4.86	2.52
Runner	3.75	1.74
Draft tube	5.00	2.27
Total	**17.70**	**9.17**

The URANS simulations were initialized with a steady solution and ran for about 400 s. A time step of 0.10224 s corresponding to 365° of runner rotation was chosen to save on computational time and resources. The four K_{WK} at $\theta = 45°$ were considered for the mesh test (figure 3). Instantaneous coefficients fluctuations along with cumulative average results are presented in the figure. Overall, the mesh test shows satisfactory results of G2 with no significant difference in average value for three of the four coefficients. However, for WK2′, the deviation is around 2%. The G1 mesh is considered in this study and a similar mesh density was also validated in a previous study [6].

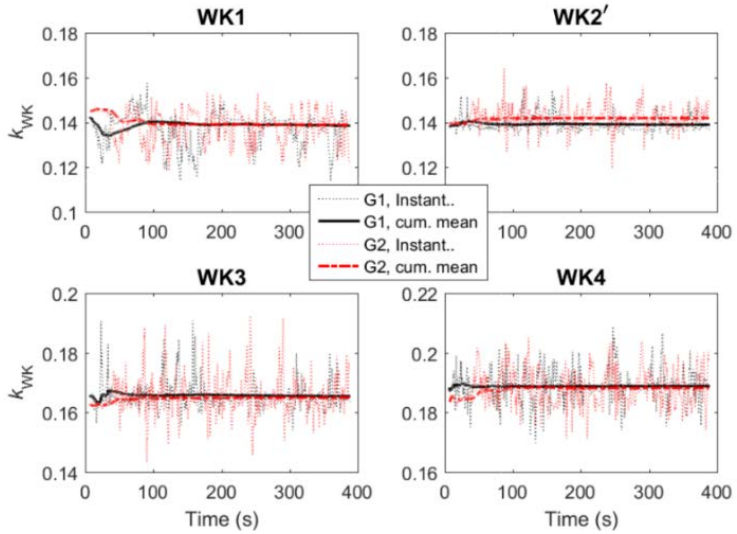

Figure 3. Grid studies for WK1-WK4 at $\theta = 45°$. G1 is finer grid and G2 is a comparatively coarse grid. Both instantaneous and cumulative average coefficients are presented. The instantaneous values show high fluctuations whereas the cumulative averaged values show satisfactory results for the two grids. The figure also shows a necessity of a longer sampling time to statistically analyze the results.

3.2. Validation studies

The comparison between K_{WK} coefficients from the numerical results and experimental data is presented in figure 4. The error bar in the figure shows the standard deviation in the data. The figure also shows the CFD result from the steady state simulation using the HP model from a previous study [6]. The numerical coefficients seem accurate for WK1 and WK4. One of the reasons that could explain why WK3 has a larger discrepancy is that the exact pressure taps location from the experiment is not known. Since the inner pressure tap ($P3$) is located near the stay vanes in a region of relatively high pressure gradient, it could be more sensitive. No data is available for WK2.

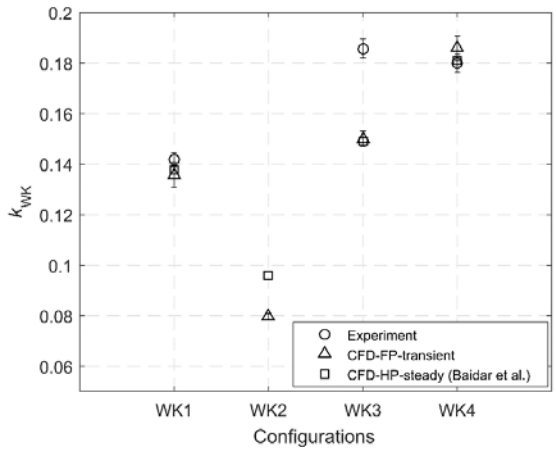

Figure 4. WK coefficients K_{WK} calculated from equation (1) for the FP model and comparison with the experimental data. The CFD-HP-steady refers to the HP model with steady simulation from Baidar et al. [6]. The error bar represents the standard deviation.

3.3. Flow behavior

The flow in the spiral casing is complex and can be influenced by the upstream geometry. For example, the upper tank considered in this study introduces some large-scale unsteadiness in the SSC elbow region as shown by the streamlines in figure 5. In the figure, the unsteadiness seems to affect the secondary flow behavior at a cross-sectional plane of the SSC as well. As we will see in the next section, this effect propagates downstream in the SSC.

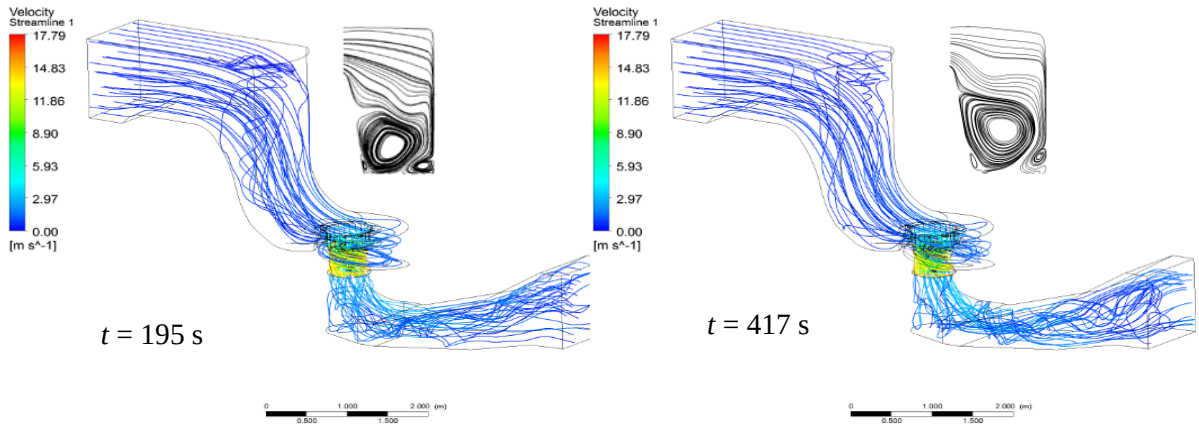

Figure 5. Velocity streamlines showing the flow condition is changing with time due to the unsteady vortex at the tank. The figure also shows the secondary flow characteristics at the cross-sectional plane of the SSC at θ =30°.

3.4. Flow distribution around the distributor

As the distributor counts 24 GVs, an ideal distribution of the flow would result in an average of 4.17% per GV sector. In figure 6(*a*), we can see that there is flow deficit at the beginning of the SSC, see sector 2-4 and some overflow in the upstream sectors: 18, 20 and 22. This trend is observed for both the FP and HP models. However, as we can see in figure 6(*b*) with an instantaneous flow distribution of the FP model at two different times, the discharge on some sectors can be affected by large scale fluctuations

coming from the intake. This is a further indication that the flow in the SSC is unsteady and can change with the inflow conditions.

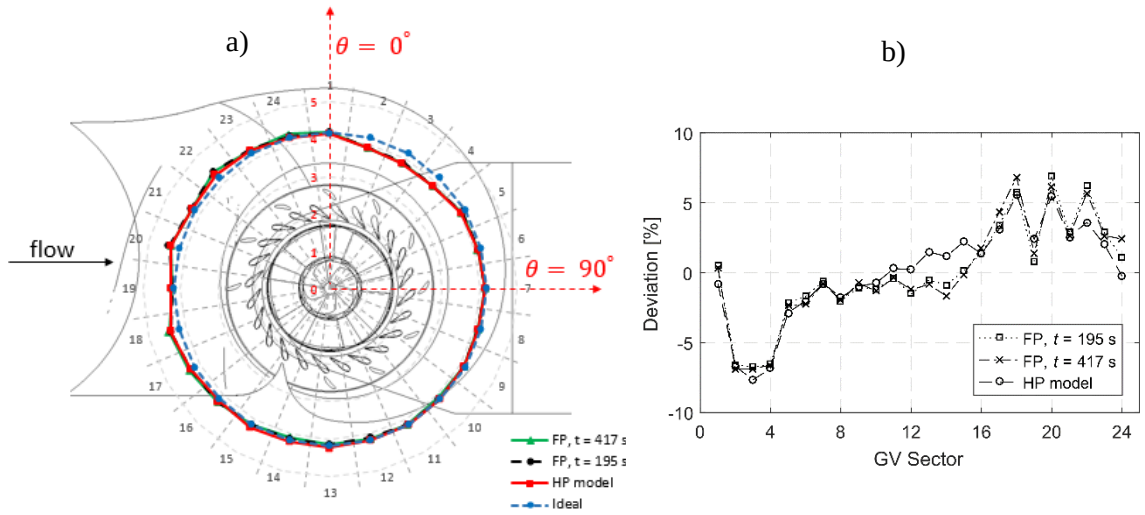

Figure 6. Normalized radial discharge in percentage from the GV sectors showing the flow distribution (*a*). The figure shows the discharge at two time instants (t = 195 s and t = 417 s) for the FP model, the HP model, and ideal flow distribution. The deviation in discharge (%) in each GV sector with respect to the ideal distribution is presented in (*b*). It indicates the flow in the SSC is unsteady and can change with inflow conditions.

A closer look at the velocity contours at the distributor central plane is presented in figure 7. The lower discharge in some sectors (2 to 4) of the SSC can be explained by the higher losses caused by large stay vane wakes. This shows that the stay vanes' profile or alignment is not optimal in this turbine.

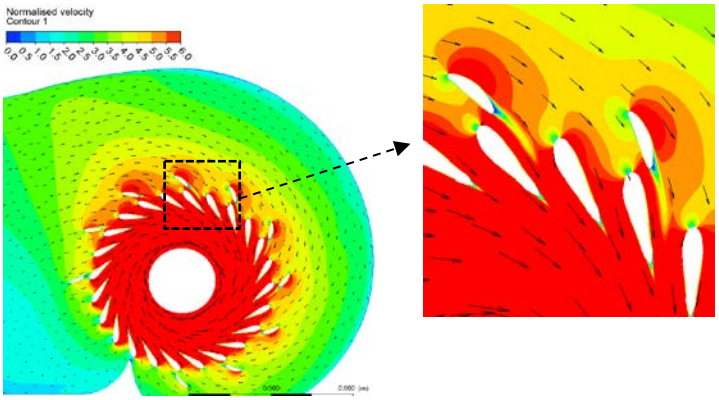

Figure 7. Contour plot in the mid-span of GV showing the velocity normalized with the bulk velocity. Velocity vectors are also presented in the figure. The figure shows the SV profile or alignment is not optimal in this turbine.

4. Effect of different runner blade angles

The effect of different runner blade angles on the WK method was studied as a mean to simulate a runner replacement. The runner at two different blade angles was considered: BEP and 5° closed position with respect to the BEP point which is termed as BEP-5°. It resulted two discharge conditions: 0.523 m^3/s for BEP and 0.425 m^3/s for BEP-5°. For both cases, the GV angle was kept constant. A constant shroud tip gap of 1.18 mm, ~ 0.9% of the blade span, was considered and 15 mesh nodes were allocated at this gap. The operating conditions for the two cases are shown in table 2. In the table, the efficiency of the turbine η and the pressure recovery factor Cp_r are defined by the following relations:

$$\eta = \frac{P_{t\_out}}{\rho g H Q} \tag{2}$$

$$Cp_r = \frac{p_{out:wall} - p_{in:wall}}{\frac{1}{2}\rho\left(Q/A_{Ia}\right)^2} \quad (3)$$

where P_{t_out} is the power output of the turbine, ρ is the water density, H is the net head. $p_{out:wall}$ is the averaged static wall pressure from 11 pressure points placed at the draft tube outlet and $p_{in:wall}$ is the averaged static wall pressure from six pressure points placed below the runner. A_{Ia} is the water passage cross-sectional area after the runner where the $p_{in:wall}$ pressure points for Cp_r are located. The exact coordinates of the pressure points that were used to calculate Cp_r may be found in Andersson et al. [9].

Table 2. Operating conditions for the study. Blade angle change case is denoted by BEP-5°. The GV angle is constant for both cases. Q, η, and Cp_r values are from numerical solution.

Operating cases	GV angle α (°)	Runner blade angle difference $\beta - \beta_{BEP}$ (°)	Discharge Q (m^3/s)	Efficiency difference $\eta - \eta_{BEP}$ (%)	Pressure recovery Cp_r (-)
BEP	29.5	0	0.523	0	0.95
BEP-5°	29.5	-5	0.425	-1.9	0.88

4.1. Time step test

Three time-steps were investigated at BEP. The time-steps correspond to 5°, 77° and 149° runner rotations. The idea behind chosen values is to utilize the expected runner blade flow passage periodicity to increase the simulation speed. Therefore, a time step of $\Delta\theta = 149°$ corresponds to 2 runner passages plus 5° and equals 41.734 ms physical time and similarly, $\Delta\theta = 77°$ corresponds to 1 runner passage plus 5° and equals 21.569 ms. The reference time step here corresponds to $\Delta\theta = 5°$ and equals 1.4 ms. Q, η, Cp_r, and four coefficients: K_{WK1} to K_{WK4} at $\theta = 45°$ were also considered, see table 3. The values were averaged over the time period equals to 38, 193 and 182 runner rotations for 5°, 77° and 149° time steps.

Table 3. Time step study in the simulation for the BEP case.

Parameters	$\Delta\theta = 149°$	$\Delta\theta = 77°$	$\Delta\theta = 5°$
Discharge, Q (m^3/s)	0.523	0.523	0.523
Efficiency, η (%)	86.7	86.9	87.2
Pressure recovery factor Cp_r (-)	0.955	0.952	0.971
K_{WK1}	0.1382	0.1383	0.1384
$K_{\mathrm{WK2'}}$	0.1376	0.1377	0.1378
K_{WK3}	0.1632	0.1632	0.1632
K_{WK4}	0.1855	0.1855	0.1855

The stabilized results of the four K_{WK} coefficients considered at $\theta = 45°$ are presented in figure 8 for 10 runner rotations. The dominant frequencies captured with $\Delta\theta = 5°$ can be related to the blade passing frequency and the rotating vortex rope (~ 0.17 runner frequency). The rotating vortex rope frequency is also noticed by using time steps equal to $\Delta\theta$ =77° and 149° in the figure. A similar rotating vortex frequency was also observed in the simulations conducted during Turbine-99 III workshop [10]. Further, the blade passing amplitude is larger when the inner pressure point is nearer to the runner, see WK2′ and WK3 in figure 8. A better convergence was achieved with the time step correspond to $\Delta\theta$ =77° than $\Delta\theta$ =149°. As the chosen time steps don't have much influence on the averaged K_{WK} coefficients, further simulations were conducted using the time step corresponding to $\Delta\theta$ =77° runner rotation to save on the computation time and resources.

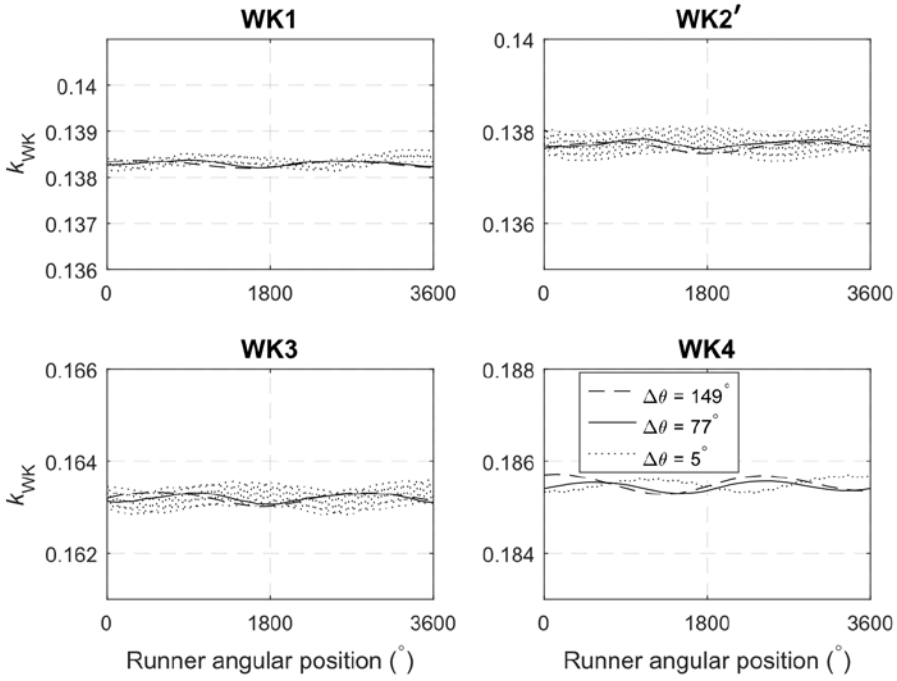

Figure 8. Time step test for the HP model for the BEP at $\theta = 45°$. The time steps ($\Delta\theta$) are presented in terms of runner rotation in degrees.

4.2. Change on the WK coefficients, K_{WK}

It was previously shown in [6] that the K_{WK} can be affected when the inlet flow condition is modified and that the various circumferential sections do not have the same level of sensitivity. The effect of different runner blade angles on the flow conditions in the SSC is studied here.

The HP model was considered using the constant head by imposing inlet total pressure. This inlet condition was generated by simulating the FP model and extracting the total pressure with velocity profile file at the inlet location of the HP model. In this way, a realistic inlet condition was achieved. The exported file was used as a total pressure inlet profile for both cases, BEP and BEP-5°. Therefore, an almost constant head was kept (some variation at the draft tube outlet can explain the offset) and the mass flow was a product of the simulation. The average net head changes between two cases is < 0.2%.

The deviation on the K_{WK} in different runner blade angle is shown in figure 9. The stable K_{WK} coefficients were averaged for about 8.45 s which corresponds to about 83 runner rotations. The averaging was done to account the periodic fluctuation of the coefficients (shown in figure 8). The deviation of the K_{WK} is < 0.5% until $\theta = 45°$ for all the considered configurations. However, the deviation increases towards the later part of the SSC (as θ increases) for WK1 and WK4. There is still a small deviation (< 0.5%) for WK2′ and WK3.

To understand how the flow changes along the θ in the SSC, the average flow characteristics at the cross-sections in the SSC (shown in figure 2) from $\theta = 0°$ to 120° for the two considered cases are shown in figure 10(*a*) and 10(*b*). The figures are presented in the form of the normalized total pressure P^* and the normalized static pressure p^*, given by equations (4) and (5):

$$P^* = \frac{\bar{\bar{P}} - P_{inlet}}{{}^1/_2 \rho v_0^2} \tag{4}$$

$$p^* = \frac{p - P_{inlet}}{{}^1/_2 \rho v_0^2} \tag{5}$$

where, $\bar{\bar{P}}$ is the mass flow averaged total pressure, P_{inlet} is the total pressure at the inlet, p is the average static pressure and v_0 is the bulk velocity for the respective case. Figure 10(a) shows a larger deviation in the total pressure as θ increases, noticeably after $\theta = 60°$. It shows there is a higher loss at BEP-5° case compared to the BEP case, as the flow is departing from the BEP condition. The static pressure also shows larger deviation as θ increases, figure 10(b).

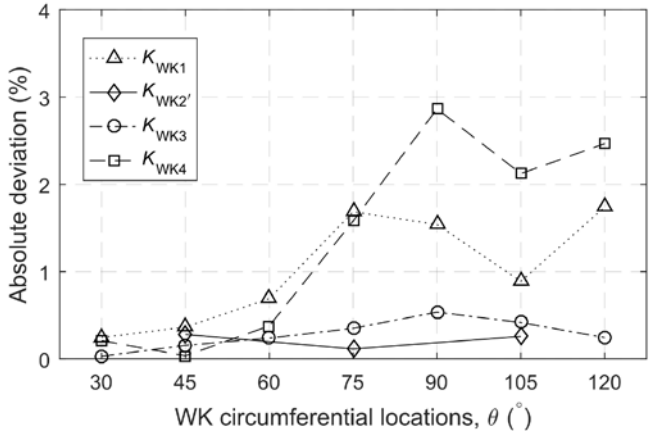

Figure 9. Absolute deviation on the K_{WK} at BEP-5° runner blade position with respect to BEP. The figure shows that there is larger deviation towards the later part of the SSC for WK1, WK3, and WK4. WK2′ and WK3 still show lesser deviation compared to WK1 and WK4. The figure suggests a better place to install WK pressure taps would be at the beginning of the SSC.

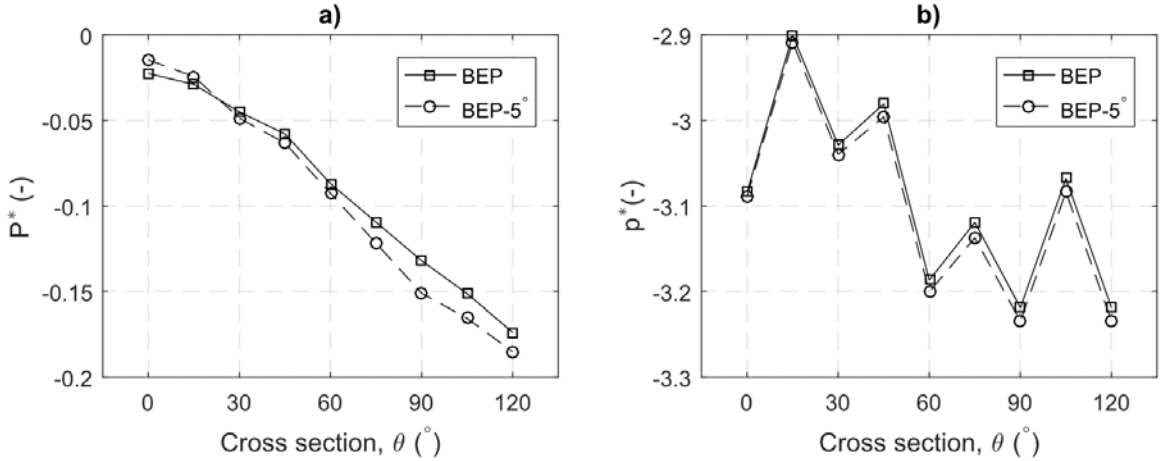

Figure 10. Average flow characteristics for BEP and BEP-5° in the cross-section from $\theta = 30°$ to 120° of the SSC. P^* shown in (a) and p^* shown in (b) represent the normalized total pressure and the normalized static pressure according to equations (4) and (5), respectively. Some changes in the total pressure and static pressure are noticed at the later part of the SSC.

The flow changes at the respective WK lines, shown in figure 2(b), at $\theta = 30°$ and $\theta = 90°$ are considered to study why the K_{WK} coefficients have larger deviation as θ increases. Figure 11(a-c) shows the pressure distribution along the lines corresponding to WK3, WK1 and WK4. The pressure distribution does not change much for line $P35$ and line $P15$, see figure 11(a) and (b) respectively. However, for line $P47$ at $\theta = 90°$, the pressure shows some changes in the inner side of the SSC, i.e. when $r^* \to 0$ in the right-hand side plot of figure 11(c). The changes in pressure can be explained by the velocity distribution shown in figure 12(a-c). The velocity components: axial v_a, radial v_r and tangential v_θ, show a similar distribution at the considered WK lines for $\theta = 30°$, whereas, for $\theta = 90°$ some changes in the velocity distribution is particularly seen for line $P47$, see v_a and v_θ distribution when $r^* \to 0$ in figure 12(c). It signifies that the flow distribution can change in the SSC with different propeller configurations and hence affect the pressure distribution.

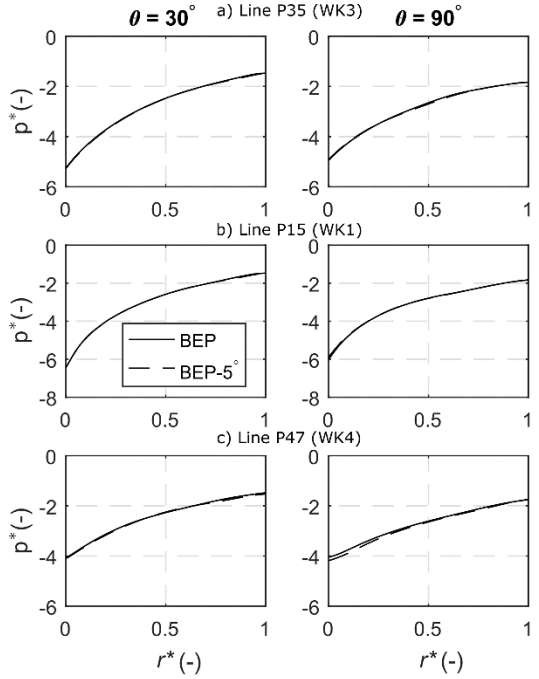

Figure 11. Pressure distribution along the respective WK lines for line $P35$ (a), line $P15$ (b) and line $P47$ (c) at $\theta = 30°$and $\theta = 90°$. The dimensionless radius r^* is given by $r^* = (r - r_i/r_o - r_i)$, where r_i is the radial coordinate at the inner wall and r_o is the radial coordinate at the outer wall of the SSC where pressure points are located.

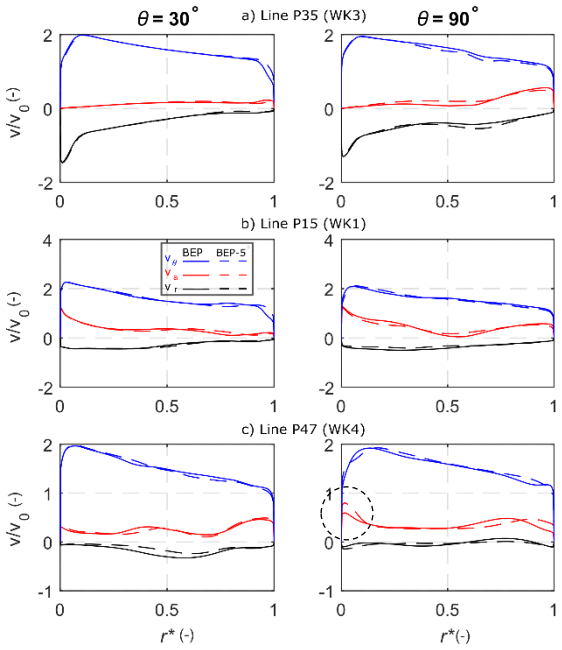

Figure 12. Axial v_a, radial v_r and tangential v_θ velocity distribution at respective WK configurations for line $P35$ (a), line $P15$ (b) and line $P47$ (c) at θ =30° and $\theta = 90°$. v_0 is the bulk velocity for the respective cases. The axial velocity distribution shows some noticeable changes between the two cases for line $P47$ towards $r^* \to 0$, marked with the dashed-circle in (c).

Furthermore, to verify whether the effects of runner blade angle change shown above was due to the imposed inlet condition in the HP model, the FP model was simulated. A time step of $\Delta\theta = 365°$ (one runner rotation plus 5°) corresponding to 0.102241 s physical time for both cases. Since time step test was not conducted for this FP model, the HP model results were presented. However, the obtained results from the FP model showed that the coefficients follow a similar trend and the conclusions drawn with the HP model are still valid.

5. Conclusion

The results showed that the flow is unsteady in the spiral casing and the WK coefficient oscillates with high amplitude. The flow distribution around the runner changes with respect to time and with different inlet conditions. This suggests that slight modifications to inlet profile can be a prime factor in anomaly reported on the WK measurement. Furthermore, the study also showed that a long sampling time is required to statistically analyze the results. The second part of the study was focused on how the change in runner blade angle, a different propeller configuration, could affect the WK method. The study showed that the flow distribution and thus the WK coefficient was altered mainly in the later part of SSC, i.e. at higher θ. Therefore, it would be better to place WK pressure taps at the beginning of SSC.

Further research is required to see if the various findings presented in this paper are general to the WK method or are specific to this geometry.

Acknowledgement

The research presented was carried out as a part of 'Swedish Hydropower Centre- SVC" and supported by the "Swedish strategic research program StandUp for Energy. SVC has been established by the

Swedish Energy Agency, Elforsk and Svenska Kraftnät together with Luleå University of Technology, The Royal Institute of Technology (KTH), Chalmers University of Technology, and Uppsala University (www.svc.nu).

References

[1] International Hydropower Association (IHA) 2017 *Hydropower Status Report* (IHA) p 5
[2] International Electrotechnical Commission 1991 IEC 60041:1991 *Field Acceptance Tests to Determine the Hydraulic Performance of Hydraulic Turbines, Storage Pumps and Pump Turbines* (Geneva: IEC)
[3] Baidar B, Nicolle J, Trivedi C and Cervantes M J 2016 Winter-Kennedy method in hydraulic discharge measurement: Problems and Challenges *11th Int. Conf. on Hydraulic Efficiency Measurement* (Linz)
[4] Kercan V, Djelic V, Rus T and Vujanic V 1996 Experience with Kaplan turbine efficiency measurements-Current meters and/or index test flow measurement *1st Int. Conf. on Hydraulic Efficiency Measurement* (Montreal)
[5] Nicolle J and Proulx G 2010 A new method for continuous efficiency measurement for hydraulic turbines *8th Int. Conf. on Hydraulic Efficiency Measurement* (Roorkee)
[6] Baidar B, Nicolle J, Trivedi C and Cervantes M J 2018 Numerical Study of the Winter-Kennedy Method - A Sensitivity Analysis *J. of Fluids Engineering* **140** 5 p 051103
[7] Lövgren M, Andersson U and Cervantes M J 2013 Some limitations of the Winter-Kennedy flow measuring method *Int. Conf. and Exhibition Hydro 2013* (Innsbruck)
[8] Menter F 1994 Two-Equation Eddy-Viscosity Turbulence Models for Engineering Applications *AIAA Journal* **32** 8 pp 1598-1605
[9] Andersson U, Engström F, Gustavsson H and Karlsson R 2004 The Turbine-99 workshops - conclusions and recommendations *22nd IAHR Symp. on Hydraulic Machinery and Systems* (Stockholm)
[10] Cervantes M J, Engström F T and Gustavsson H L 2005 *Proc. of the 3rd IAHR/ERCOFTAC Workshop on Draft tube Flows* (Luleå: Luleå University of Technology)